

# Polydisperse fluid mixtures of adhesive colloidal particles

Domenico Gazzillo<sup>1</sup> and Achille Giacometti

*INFN and Dipartimento di Chimica Fisica,  
Università di Venezia, S. Marta DD 2137, I-30123 Venezia, Italy*

---

## Abstract

We investigate polydispersity effects on the average structure factor of colloidal suspensions of neutral particles with surface adhesion. A sticky hard sphere model alternative to Baxter's one is considered. The choice of factorizable stickiness parameters in the potential allows a simple analytic solution, within the “mean spherical approximation”, for any number of components and arbitrary stickiness distribution. Two particular cases are discussed: i) all particles have different sizes but equal stickiness (Model I), and ii) each particle has a stickiness proportional to its size (Model II). The interplay between attraction and polydispersity yields a markedly different behaviour for the two Models in regimes of strong coupling (i.e. strong adhesive forces and low temperature) and large polydispersity. These results are then exploited to reanalyze experimental scattering data on sterically stabilized silica particles.

*Keywords:* Colloidal models, sticky hard spheres, polydispersity, structure factors, small angle scattering.

---

## 1 Introduction

In studies on colloidal suspensions of neutral particles with adhesive interactions [1–3], several attempts have been made to fit small angle scattering data by using Baxter's “sticky hard sphere” (SHS) model [4]. In addition to a hard sphere (HS) repulsion, the SHS potential contains a surface adhesive term, introduced by Baxter as a limit of an attractive square well which becomes infinitely deep and narrow according to a particular prescription [4]. For this model the Ornstein-Zernike (OZ) integral equations of the liquid state

---

<sup>1</sup> Corresponding author. *E-mail address:* gazzillo@unive.it

theory have been solved analytically within the Percus-Yevick (PY) approximation, and expressions for the correlation functions are thus available [4–6]. Unfortunately, however, for a fluid with  $p$  components the SHS-PY analytical solution requires the knowledge of a set of density-dependent parameters  $\lambda_{ij}$ , to be determined through  $p(p+1)/2$  coupled quadratic equations [5,6]. This feature makes Baxter’s SHS-PY solution for mixtures practically inapplicable to colloidal systems with significant polydispersity, i.e. with large  $p$ .

Polydispersity means that the mesoscopic suspended particles of a same chemical species may differ in size, charge or other properties. Consequently, a polydisperse fluid is always a mixture with a large number of components and strong asymmetries (in size, charge, etc.), even when all meso-particles belong to a unique chemical species.

In a recent paper (hereafter referred to as Reference I) [7] we showed that the aforesaid shortcomings of the SHS-PY solution can be avoided by using a different version of SHS potential, for which the OZ equations are analytically solvable under a different closure, i.e. the “mean spherical approximation” (MSA) [8–10]. In this alternative SHS model, the adhesive term is defined starting from a Yukawa attractive tail and taking the “sticky limit” of infinite amplitude and vanishing range, with their product remaining constant. In Ref. I it was pointed out how, in the particular case of *factorizable stickiness parameters* in the adhesive term, the SHS-MSA solution leads to closed analytical expressions for scattering intensity and other “global” structure factors, which are valid for *arbitrary*  $p$  and therefore are suitable to fit experimental scattering data from polydisperse systems.

In the present work we shall review the main points of Ref. I, adding some new results and remarks. We shall then apply the SHS-MSA solution to small-angle-neutron-scattering data from a colloidal fluid formed by sterically stabilized silica particles.

## 2 Model and scattering functions

Our SHS potential is defined by

$$\beta u_{ij}(r) = \beta u_{ij}^{\text{HS}}(r) - K_{ij} \sigma_{ij}^{-1} \delta_+(r - \sigma_{ij}), \quad (1)$$

with factorizable stickiness parameters [11,12]

$$K_{ij} = Y_i Y_j, \quad Y_i \geq 0, \quad (i, j = 1, \dots, p), \quad (2)$$

which measure the strength of surface attraction. In Eq. (1),  $u_{ij}^{\text{HS}}(r)$  is the HS potential and the next term stems from the “sticky limit” of a Yukawa tail [13];  $\beta = (k_B T)^{-1}$ ,  $\sigma_{ij} = (\sigma_i + \sigma_j)/2$ , with  $\sigma_i$  being the HS diameter of species  $i$ , and  $\delta_+(x)$  is the asymmetrical Dirac delta function defined by:  $\int_a^b dx f(x) \delta_+(x - c) = f(c^+)$ , if  $a \leq c < b$ . The MSA solution for this model is represented by the factor correlation functions

$$q_{ij}(r) = \begin{cases} \frac{1}{2}a_i(r^2 - \sigma_{ij}^2) + b_i(r - \sigma_{ij}) + K_{ij}, & L_{ij} \leq r \leq \sigma_{ij} \\ 0, & \text{elsewhere} \end{cases} \quad (3)$$

where  $L_{ij} = (\sigma_i - \sigma_j)/2$  and the expressions of  $a_i$  and  $b_i$  can be found in Ref. I. Once that the  $q_{ij}(r)$  are known, all correlation and scattering functions are in principle computable. The *partial* structure factors are given by [7,15]

$$S_{ij}(k) = \sum_{m=1}^p \hat{Q}_{im}^{-1}(k) \hat{Q}_{jm}^{-1}(-k), \quad (4)$$

where  $\hat{Q}_{ij}(k) = \delta_{ij} - 2\pi(\rho_i \rho_j)^{1/2} \hat{q}_{ij}(k)$ , with  $\hat{q}_{ij}(k)$  being the unidimensional Fourier transform of  $q_{ij}(r)$  ( $\delta_{ij}$  the Kronecker  $\delta$ ,  $\rho_i$  the number density of species  $i$ ). The scattering intensity as well as other *global* structure factors can then be calculated, all these scattering functions being weighted sums of  $S_{ij}(k)$ , like  $\sum_{i,j=1}^p w_i(k) w_j^*(k) S_{ij}(k)$  (here, the asterisk means complex conjugation). As an example, we mention the *measurable average structure factor*

$$S_M(k) = \sum_{i,j=1}^p (x_i x_j)^{1/2} F_i(k) F_j^*(k) S_{ij}(k) / \sum_{i=1}^p x_i |F_i(k)|^2, \quad (5)$$

where  $x_i$  is the molar fraction of species  $i$  and  $F_i(k)$  its form factor. Eq. (4) shows that the main difficulty in the computation of  $S_{ij}(k)$  lies in the inversion of a  $p \times p$  matrix  $\hat{\mathbf{Q}}(k)$ , which usually becomes a formidable task with increasing  $p$ . Nevertheless, as discussed in Ref. I, when  $K_{ij}$  is factorizable as in Eq. (2),  $\hat{\mathbf{Q}}(k)$  becomes a *dyadic* (or Jacobi) matrix, i.e.  $\hat{Q}_{ij}(k) = \delta_{ij} + \sum_{\mu=1}^n a_i^{(\mu)}(k) b_j^{(\mu)}(k)$ , which admits *analytic* inverse for *any*  $p$  (in general, the same property does not hold for Baxter’s SHS-PY solution [14]). Another important consequence of the dyadic structure is that it allows to compute the *global* scattering factors *bypassing* a preliminary calculation of the individual  $S_{ij}(k)$ . Indeed, when  $\hat{\mathbf{Q}}(k)$  is dyadic the sums  $\sum_{i,j=1}^p w_i(k) w_j^*(k) S_{ij}(k)$  can be worked out analytically (see Refs. [7,15,16] for details), unlike the most common case where they are performed numerically by evaluating  $p(p+1)/2$  independent contributions  $S_{ij}(k)$  at each  $k$ . When fitting experimental data, the availability of closed analytical expressions directly for scattering intensity and  $S_M(k)$  clearly represents a great advantage.

### 3 Polydispersity effects in SHS fluids

#### 3.1 Size and stickiness distributions

To represent size polydispersity, we select  $p$  possible diameters uniformly distributed in an interval  $(0, \sigma_{\max})$  with mesh size  $\Delta\sigma = 0.02 \langle\sigma\rangle$ . Each diameter  $\sigma_i$  characterizes a different component. Its molar fraction is  $x_i = f(\sigma_i)\Delta\sigma$ , with  $f$  expressed by a Schulz distribution, i.e.

$$f(\sigma) = b^a \sigma^{a-1} e^{-b\sigma} / \Gamma(a) \quad (a > 1), \quad (6)$$

where  $\Gamma$  is the gamma function,  $\langle\sigma\rangle$  the average diameter,  $a = 1/s_\sigma^2$ ,  $b = a/\langle\sigma\rangle$  and  $s_\sigma = [\langle\sigma^2\rangle - \langle\sigma\rangle^2]^{1/2}/\langle\sigma\rangle$  measures the degree of size polydispersity. We use  $p = 85$  components when  $s_\sigma = 0.1$ , and  $p = 175$  when  $s_\sigma = 0.3$ .

The model can in principle be worked out for any choice of  $Y_i$ , which meets the requirements that  $Y_i$  must be lengths and  $K_{ij} = Y_i Y_j$  must be proportional to  $\beta = (k_B T)^{-1}$ . However, two choices are particularly interesting:

**Model I** (*polydisperse in size but monodisperse in stickiness*), which assumes that all particles have the same stickiness, i.e.

$$Y_i = Y = \gamma_0 \langle\sigma\rangle, \quad \text{with} \quad \gamma_0^2 = \frac{\varepsilon_0}{k_B T} = \frac{1}{T^*}. \quad (7)$$

Here,  $\gamma_0$  measures the strength of surface adhesion;  $\varepsilon_0$  is an energy, and  $T^*$  a reduced temperature. High  $T^*$  (low  $\gamma_0$ ) values correspond to weak surface adhesion or high temperature; vice versa, low  $T^*$  (high  $\gamma_0$ ) values mean strong attraction or low temperature.

**Model II** (*with stickiness polydispersity linearly related to the size one*). Since it is reasonable to expect that larger particles attract each other more strongly, a simple way of introducing stickiness polydispersity is the choice

$$Y_i = \gamma_0 \sigma_i. \quad (8)$$

#### 3.2 Regimes for $S_M(k)$ and generalized Boyle temperature

Polydispersity effects on  $S_M(k)$  can be best described after recalling some features of the monodisperse SHS structure factor.

In  $S_{\text{mono}}(k)$  the presence of strong adhesive forces may be revealed mainly from its behaviour in the low- $k$  region. Here,  $S_{\text{mono}}^{\text{SHS}}(k)$  may differ significantly from  $S_{\text{mono}}^{\text{HS}}(k)$ , exhibiting a drastic increase as  $k \rightarrow 0$  (see Figure 1 for  $s_\sigma = 0$ ). More precisely, in Ref. I we recognized the existence of two different “regimes” for  $S_{\text{mono}}^{\text{SHS}}(k)$  respectively above and below the *Boyle temperature*,  $T_B^* = 3$ , where attractive and repulsive forces balance each other in such a way that  $B_2$  vanishes (the second virial coefficient  $B_2$  appears in the low-density expansion of  $S_{\text{mono}}(0) = 1 - 2B_2(T^*)\rho + \mathcal{O}(\rho^2)$ ). When  $T^* > T_B^*$  ( $B_2 > 0$ ) the fluid behaves like pure HS without stickiness, repulsive forces are dominant, and  $S_{\text{mono}}(0)$  - which is related to compressibility and density fluctuations - decreases with increasing volume fraction  $\eta$ . When  $T^* < T_B^*$  ( $B_2 < 0$ )  $S_{\text{mono}}(0)$  has a non-monotonic dependence on  $\eta$ . After an initial increase (which may become very strong, signalling the approach to a gas-liquid phase transition with critical temperature  $T_c^* \simeq 1.61$ ), an inversion occurs and  $S_{\text{mono}}(0)$  decreases with  $\eta$ . In other words, below  $T_B^*$  the attractive forces are dominant at low  $\eta$ , whereas repulsion prevails at higher  $\eta$ .

For polydisperse SHS, there exist two similar “regimes” for  $S_M(k)$ . The new feature is that a crossover between these regimes can now be induced not only by a change of  $T^*$ , but also by a change of polydispersity  $s_\sigma$  (at fixed  $T^*$ ).

Figure 1 illustrates the polydispersity effects on  $S_M(k)$ , displaying its behaviour at  $T^* = 2.04$  ( $\gamma_0 = 0.7$ ) and  $\eta = 0.2$ , as  $s_\sigma$  increases from 0 (monodisperse limit) to 0.1 and 0.3. We employed form factors  $F_i(k)$  for homogeneous spherical scattering cores inside the particles, with scattering core diameters  $\sigma_i^{\text{scatt}}$  coincident with the HS ones, i.e.  $\sigma_i^{\text{scatt}} = \sigma_i$ . Polydispersity progressively dumps all oscillations in the first peak region and beyond. Here, Model I and II are nearly equivalent, whereas their  $S_M(k)$  may strongly differ near the origin as a consequence of the different stickiness distributions. In fact, increasing  $s_\sigma$  (at the fixed  $T^*$  value) does not produce marked differences in Model II. On the contrary, in Model I a large polydispersity can overwhelm the attractive effects, leading to a strong HS-like decrease of  $S_M(0)$  and thus preventing the possibility of an instability in the system.

In Ref. I this scenario was interpreted in terms of a *generalized Boyle temperature*,  $T_{B,F}^*$ . From the low-density expansion of  $S_M(0) = 1 - 2B_{2,F}(T^*)\rho + \mathcal{O}(\rho^2)$ , we derived  $B_{2,F}$  as a generalization of  $B_2$  when all form factors are included. Then  $B_{2,F}(T_{B,F}^*) = 0$  defines  $T_{B,F}^*(s_\sigma)$ , which is a decreasing function of  $s_\sigma$  (its expression is given in Ref. I). Clearly,  $T_{B,F}^*(s_\sigma = 0) = (T_B^*)_{\text{mono}} = 3$ . In a  $(s_\sigma, T^*)$  diagram, above the curve  $T^* = T_{B,F}^*(s_\sigma)$  there is the region corresponding to a “HS-like, repulsive regime”; below, there is the “attractive-regime” region. Now, as shown in the inset of Figure 1,  $T_{B,F}^*(s_\sigma)$  of Model II decreases very slowly, asymptotically approaching 2.57; therefore, all three  $(s_\sigma, T^* = 2.04)$ -states of Figure 1 lie in the lower region. On the other hand,  $T_{B,F}^*(s_\sigma)$  of Model I is a rapidly decreasing function, with  $T_{B,F}^*(s_\sigma = 0.1) = 2.79 > T^*$

and  $T_{B,F}^*(s_\sigma = 0.3) = 1.68 < T^*$ . This argument interprets the crossover from “attractive” to “repulsive” regime in terms of an increasing polydispersity.

## 4 Fit of experimental data

To investigate polydispersity effects in real colloidal fluids, we now apply our Models to experimental data for silica particles coated with octadecyl chains and dispersed in benzene. For this system Duits *et al.* [3] published a wide set of small-angle neutron-scattering results, which exhibit a crossover from “HS-like repulsive” to “attractive” regime controlled by variation of  $T$ : on lowering the temperature, attractive effects increase and a reversible phase separation into two phases of different density occurs at  $t = 32.5$  °C. Duits *et al.* [3] fitted their experimental data using an implementation by Robertus *et al.* [1] of Baxter’s SHS-PY model, with stickiness independent of size and size polydispersity represented by a rather limited number of components (up to  $p = 9$ ), due to the aforesaid shortcomings of the PY solution. The form factors  $F_i(k)$  were calculated with a model of spherical three-layer particles, and a difference between HS and scattering core diameters, with  $\sigma_i > \sigma_i^{\text{scatt}}$ , was admitted.

Since our aim is not an exhaustive analysis of all data by Duits *et al.* [3], in Figure 2 we consider only two representative cases, with  $\eta = 0.28$  and  $t = 51.6$  °C and  $35.4$  °C, respectively. The  $S_M(k)$  of the first sample (Figure 2a) is typically “HS-like”, whereas at low  $k$  the curve of Figure 2b has an upswept shape characteristic of strong attraction. For simplicity, we calculate the form factors with a model of homogeneous spherical scattering cores. We have checked that this choice is essentially equivalent to the three-layer one, if appropriate average contrast and diameter (  $\langle \sigma^{\text{scatt}} \rangle = 39.8$  nm ) are used, as suggested by Ref. [3].

In Figure 2a we first fit the experimental data by employing the monodisperse SHS-MSA model (all particles having the same size and stickiness;  $s_\sigma = 0$ ), with two free parameters,  $T^*$  and  $\sigma > \langle \sigma^{\text{scatt}} \rangle$ . The best fit results are:  $(T^*, \sigma) = (4.2, 45.6)$ , with the value of  $T^*$  confirming that the system is in the “repulsive” regime. Clearly, this model overestimates the first peak height and does not reproduce the rising part of the curve adequately. Both these drawbacks can be overcome by taking size polydispersity into account. Indeed, both Model I and II yield excellent agreement, and their results are nearly identical, indicating that the choice of stickiness distribution is irrelevant in this HS-like case. To use only two free parameters, i.e.  $\langle \sigma \rangle > \langle \sigma^{\text{scatt}} \rangle$  and  $s_\sigma$ , for Model I and II we fix  $T^*$  on the value found with the monodisperse model. The best fit results are:  $(\langle \sigma \rangle, s_\sigma) = (44.9, 0.12)$  for Model I, and  $(44.2, 0.15)$  for Model II (using three free parameters, i.e.  $T^*, \langle \sigma \rangle, s_\sigma$ , does

not alter our qualitative results). We remark that both our estimates of  $s_\sigma$  are consistent with the value 0.11 of Ref. [3]. Moreover, comparison with Figure 6 of Ref. [3] shows that Model I improves over its PY counterpart of Duits *et al.* This may be due to our use of a much larger number  $p$  of components to represent the size distribution.

In Figure 2b we use a similar strategy. Here, however, we have found impossible to satisfactorily fit the entire experimental curve with the monodisperse model. Hence, we have forced  $T^*$  to the value 2.3 which best reproduces the data within the restricted  $k$ -range (0.03, 0.15) nm<sup>-1</sup> (note that this value of  $T^*$  indicates that the system is in the “attractive” regime). Then, upon fitting the complete set of data with one free parameter, we find  $\langle\sigma\rangle = 43.0$  nm for the monodisperse model. On fixing  $T^* = 2.3$ , the best results for Model I and II are:  $(\langle\sigma\rangle, s_\sigma) = (41.9, 0.12)$  and  $(41.5, 0.13)$ , respectively. Once again we note the importance of the polydispersity effects, which lower the first peak height correctly and improve the general agreement. Both Models are satisfactory, although Model II appears to be slightly superior, indicating, perhaps, that the difference of stickiness distribution is already becoming significant. However, this conclusion cannot be definitive. In fact, further calculations (not reported here) under different conditions, yield ambiguous results. Moreover, Figure 1 shows that the differences between Model I and II are small at low  $s_\sigma$  values, as unfortunately occurs in the colloidal system investigated by Duits *et al.* [3]. On the other hand, our results suggest the opportunity of further experimental investigations on similar fluids with larger polydispersity, where an analysis of  $S_M(k)$  at low  $k$  could discriminate between different SHS Models and provide useful information about the unknown real stickiness distribution.

## 5 Conclusions

The present study on a new polydisperse SHS model has once again shown the importance of taking polydispersity effects into account when experimental scattering data are analyzed. We have found that even a small degree of size polydispersity,  $s_\sigma \simeq 0.1$ , can strongly modify  $S_M(k)$  with respect to the monodisperse case. We have pointed out the existence of “repulsive” and “attractive” regimes for  $S_M(k)$ , with a crossover interpreted in terms of a “generalized Boyle temperature”, dependent on the degree of polydispersity. In the presence of polydispersity, a crossover between these regimes can be induced not only by a change of  $T^*$ , but also by a change of  $s_\sigma$  (at fixed  $T^*$ ).

In addition to size polydispersity, we have considered two simple stickiness distributions (Model I and II). Our results indicate that the particular choice of stickiness distribution is irrelevant in fluids with small size polydispersity and weak coupling (i.e. weak attraction and high temperature). On the contrary,

stickiness polydispersity effects can be revealed from the low- $k$  behaviour of  $S_M(k)$  when size polydispersity is large and coupling is strong (strong adhesive forces and low temperature).

As an application, we have employed Model I and II to analyze experimental scattering data for a colloidal fluid with short-range attractions. Our best fit results are satisfactory and suggest the importance of the stickiness polydispersity (Model II). However, the considered experimental system lies in a regime where it is impossible to unambiguously discriminate between our two Models. New scattering studies on fluids with larger size polydispersity and stronger adhesive forces would be desirable to get more insight into this problem.

## Acknowledgements

Partial financial support by the Italian INFN (Istituto Nazionale di Fisica della Materia) is gratefully acknowledged.

## References

- [1] C. Robertus, W. H. Philipse, J. G. H. Joosten and Y. K. Levine, *J. Chem. Phys.* 90 (1989) 4482.
- [2] M. H. G. Duits, R. P. May, and C. G. de Kruif, *J. App. Crist.* 23 (1990) 366.
- [3] M. H. G. Duits, R. P. May, A. Vrij, and C. G. de Kruif, *Langmuir* 7 (1991) 62.
- [4] R. J. Baxter, *J. Chem. Phys.* 49 (1968) 2270.
- [5] J. W. Perram and E. R. Smith, *Chem. Phys. Lett.* 35 (1975) 138.
- [6] B. Barboy and R. Tenne, *Chem. Phys.* 38 (1979) 369.
- [7] D. Gazzillo, and A. Giacometti, *J. Chem. Phys.* 113 (2000) 9846.
- [8] J. J. Brey, A. Santos and F. Castano, *Mol. Phys.* 60 (1987) 113.
- [9] L. Mier-y-Teran, E. Corvera and A. E. Gonzalez, *Phys. Rev. A* 39 (1989) 371.
- [10] C. Tutschka and G. Kahl, *J. Chem. Phys.* 108 (1998) 9498.
- [11] M. Yasutomi and M. Ginoza, *Mol. Phys.* 89 (1996) 1755.
- [12] J. N. Herrera, L. Blum and P. T. Cummings, *Mol. Phys.* 93 (1998) 73.
- [13] M. Ginoza and M. Yasutomi, *Mol. Phys.* 87 (1996) 1755.
- [14] J. N. Herrera and L. Blum, *J. Chem. Phys.* 94 (1991) 6190.
- [15] D. Gazzillo, A. Giacometti and F. Carsughi, *J. Chem. Phys.* 107 (1997) 10141.
- [16] A. Vrij, *J. Chem. Phys.* 69 (1978) 1742; *ibidem* 71 (1979) 3267.



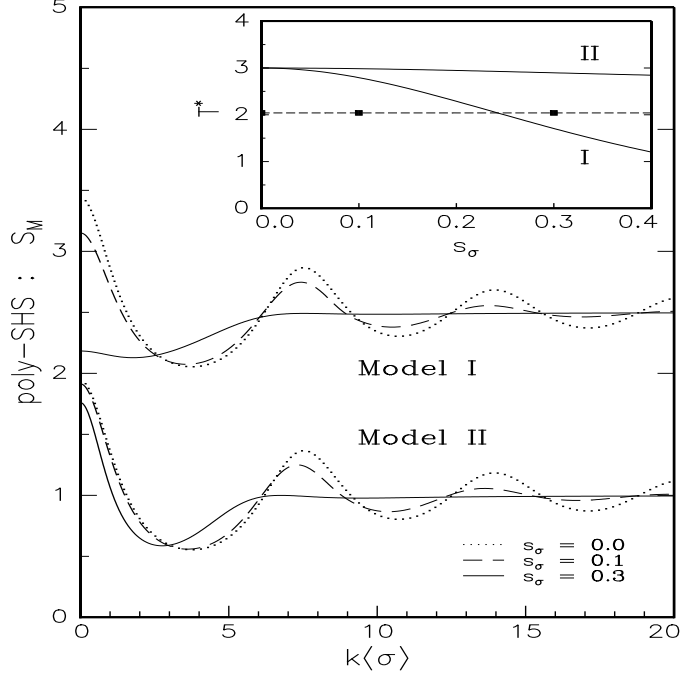


Fig. 1. Structure factor  $S_M(k)$  of the SHS-MSA Models I and II at  $T^* = 2.04$  and  $\eta = 0.2$ , for several degrees of polydispersity  $s_\sigma$  (the curves of Model I are shifted upwards by 1.5 units to avoid overlapping). In the inset, the solid curves represent  $T_{B,F}^*(s_\sigma)$  of the two Models, the dashed line corresponds to the isotherm  $T^* = 2.04$  and the black squares on it are the considered states.

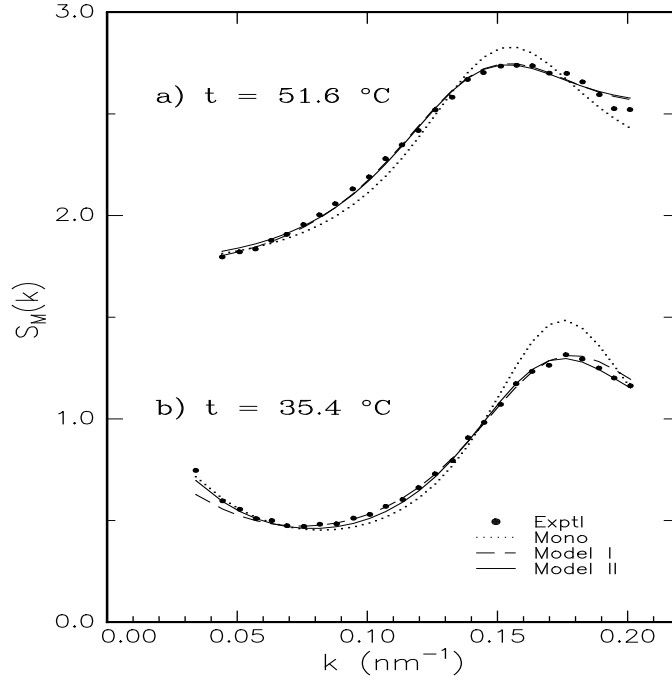


Fig. 2. Fit of experimental neutron scattering data for  $S_M(k)$  at  $\eta = 0.28$  and two different temperatures (taken from Ref. [3]), by using monodisperse and polydisperse SHS-MSA models (the curves of part (a) are shifted upwards by 2.5 units).